Available online at www.sciencedirect.com
SCIENCE DIRECT®
Journal of Catalysis 225 (2004) 359–368
JOURNAL OF CATALYSIS
www.elsevier.com/locate/jcat

Use of kinetic models to explore the role of base promoters on Ru/MgO ammonia synthesis catalysts

Stacey E. Siporin and Robert J. Davis *

Department of Chemical Engineering, University of Virginia, Charlottesville, VA 22904-4741, USA

Received 12 November 2003; revised 29 March 2004; accepted 31 March 2004

Available online 25 May 2004

Abstract

The kinetics of ammonia synthesis over unpromoted and Cs-, Ba-, and La-promoted Ru/MgO (∼ 2 wt%) were studied in a tubular reactor at 20.7 atm. The reaction over all of the catalysts was nearly first order in N_2 and nearly zero order in NH_3. However, the order of reaction in H_2 was largely dependent on the choice of promoter, with Ba and La significantly reducing the inhibition by dihydrogen seen on Cs-promoted Ru/MgO. The turnover frequencies on Ba- and La-promoted Ru/MgO under stoichiometric conditions and 673 K were almost an order of magnitude greater than that on Cs-promoted Ru/MgO. Two kinetic models with optimized parameters were used to describe the outlet ammonia pressures determined experimentally both close to and far from equilibrium. Although Cs promotion of Ru lowered the activation barrier for N_2 dissociation, the enthalpy of dihydrogen adsorption and therefore the H atom surface coverage increased. Thus, promotion of Ru catalysts with bases cannot be attributed solely to an effect on dinitrogen dissociation, which is the rate-determining step. Base promotion is a trade-off between lowering the activation barrier for N_2 dissociation and increasing the competitive adsorption of H_2. The coverages of nitrogen-containing species determined by an optimized kinetic model matched well those determined experimentally by isotopic transient analysis over the same catalysts.

Keywords: Kinetic modeling; Ammonia synthesis; Promotion of ruthenium; Cesium; Barium; Lanthanum; Magnesium oxide

1. Introduction

Ruthenium-based materials are the second-generation catalysts for ammonia synthesis. Ruthenium is less inhibited by ammonia, less sensitive to poisons, and more active than the traditional iron-based catalyst [1]. The relatively high cost of Ru compared to iron requires a high dispersion of the metal on a suitable support.

The Ocelot Ammonia Plant in British Columbia utilizes a carbon-supported Ru catalyst [2]. A significant reduction of energy consumption was observed with the incorporation of this new catalyst; however, Ru is also known to catalyze carbon gasification [3,4]. Thus, the lifetime of carbon-supported Ru catalysts may impede its widespread use [5]. Nonreducible metal oxides are therefore being explored as potential supports for Ru.

Without the addition of basic promoters, Ru has very little catalytic activity for ammonia synthesis [6–43]. Generally, highly basic promoters such as alkali metal oxides or hydroxides are the best. It is quite interesting that less basic alkaline earth and lanthanide promoters such as Ba and La oxides or hydroxides effectively promote Ru for ammonia synthesis [6,8–12,14,18–22,24,25,27,28,30–41,43].

One significant difference between the kinetics of ammonia synthesis over Ru and Fe is the dependence of the rate on H_2 pressure. Typically, Ru catalysts are strongly inhibited by dihydrogen, with the order of reaction often approaching −1, whereas over Fe the reaction order in dihydrogen is positive [1,11,26]. The negative dihydrogen order for Ru catalysts suggests that the catalysts should be operated at the less thermodynamically favorable nonstoichiometric conditions. A supported Ru catalyst that is less inhibited by H_2 is therefore highly desirable.

Lanthanide supports and promoters decrease the inhibition by H_2 [19–24,27,43]. For example, we have recently shown that lanthanum promotion of Ru on zeolitic sup-

* Corresponding author.
E-mail address: rjd4f@virginia.edu (R.J. Davis).

0021-9517/$ – see front matter
doi:10.1016/j.jcat.2004.03.046

ports nearly eliminates dihydrogen inhibition during ammonia synthesis at a total pressure of 20.7 atm. An alkaline earth promoter such as Ba has also reduced the H_2 inhibition during ammonia synthesis on Co, Co–Fe alloys, Ru/MgO and Ru/C catalysts [41–43].

In a previous paper, we reported on the use of isotopic transient analysis to investigate the global and intrinsic kinetics of La-, Ba-, or Cs-promoted Ru/MgO under ammonia synthesis conditions [41]. Steady-state, global measurements revealed that Cs–Ru/MgO was strongly inhibited by dihydrogen whereas Ba–Ru/MgO and La–Ru/MgO were weakly inhibited by the reactant at 3 atm total pressure. Based on intrinsic activity measurements from isotopic transient analysis, Cs-promoted Ru/MgO was twice as active than either Ba- or La-promoted Ru/MgO [41]. However, the coverage of nitrogen-containing species was significantly higher on the Ba- and La-promoted catalysts compared to Cs–Ru/MgO. Therefore there was a trade-off between NH_x coverage and intrinsic activity of the promoted samples. Similar results were found in our analogous study of Cs- or Ba-promoted Ru/C catalysts [43]. For base promoted Ru, the global rate was strongly influenced by the competitive adsorption of dihydrogen [41]. An optimally promoted catalyst would strike an appropriate balance between inhibition by dihydrogen and enhancement of dinitrogen dissociation.

Two types of models have been used to describe the kinetics of ammonia synthesis on Ru catalysts supported on nonreducible oxides [12,16,29]. The simplest one assumes that dissociative adsorption of dinitrogen is the rate-determining step and the only intermediates present on the surface in kinetically significant amounts are N and H atoms [12]. Adsorption of H_2 and subsequent hydrogenation steps are assumed to be quasi-equilibrated. This model is depicted in Mechanism 1:

$$H_2 + 2* \rightarrow 2H*, \tag{1a}$$

$$N_2 + 2* \underset{k_4}{\overset{k_3}{\rightleftarrows}} 2N*, \tag{1b}$$

$$N* + 3H* \underset{k_6}{\overset{k_5}{\rightleftarrows}} NH_3 + 4*, \tag{1c}$$

where $*$ denotes an active site on the catalyst surface. Previous results from parameter optimization of catalysts with strong dihydrogen inhibition indicated that the most active catalysts reduced the activation energy for dinitrogen dissociation while the enthalpy of dihydrogen adsorption was approximately 75 kJ mol^{-1} [12].

A second more complex model was utilized by Hinrichsen et al. [16] and Dahl et al. [29]. The reaction sequence, shown in Mechanism 2, accounts for all of the elementary steps on the surface. It allows for N, H, NH, NH_2, and NH_3 to be present on the surface in kinetically significant amounts.

$$H_2 + 2* \rightarrow 2H*, \tag{2a}$$

$$N_2 + 2* \underset{k_4}{\overset{k_3}{\rightleftarrows}} 2N*, \tag{2b}$$

$$N* + H* \underset{k_6}{\overset{k_5}{\rightleftarrows}} NH* + *, \tag{2c}$$

$$NH* + H* \underset{k_8}{\overset{k_7}{\rightleftarrows}} NH_2* + *, \tag{2d}$$

$$NH_2* + H* \underset{k_{10}}{\overset{k_9}{\rightleftarrows}} NH_3* + *, \tag{2e}$$

$$NH_3* \underset{k_{12}}{\overset{k_{11}}{\rightleftarrows}} NH_3 + *. \tag{2f}$$

The research groups used results from single-crystal surface science studies as well as fundamental studies on $Ru/MgAl_2O_4$ and Cs–Ru/MgO catalysts to obtain the activation energies and preexponential factors of some of the elementary steps. Large data sets obtained over a wide range of total pressures were used to test the model. In the paper by Dahl et al., dinitrogen dissociation was assumed to be the rate-determining step, and therefore, all subsequent steps were quasi-equilibrated [29]. Hinrichsen et al. did not assume a rate-determining step in their analysis [16].

The purpose of the current work is to use kinetic modeling of the ammonia synthesis reaction to elucidate the role of promoter on La-, Ba-, or Cs-promoted Ru/MgO catalysts. In particular, the promoter affects the global reaction rate and the order of reaction with respect to dihydrogen. The ammonia synthesis activity of each of the catalysts was tested under high-pressure conditions both close to and far from equilibrium. The activity results were used to regress the kinetic parameters associated with Mechanisms 1 and 2. In both cases, a set of continuously stirred tank reactors (CSTRs) in series was used to model the experimental tubular reactor.

2. Experimental methods

2.1. Catalyst preparation

The procedure used for catalyst preparation is described in our earlier work [41]. Briefly, the magnesia support (Ube Industries, 42 m^2 g^{-1}) was mixed with approximately 2 wt% Ru in the form of $Ru_3(CO)_{12}$ (Aldrich, 99%), dissolved in THF. After THF evaporation, the sample was heated in vacuum to 723 K and held at temperature for 2 h and cooled. The sample was then reduced in dihydrogen at 723 K for 1 h, evacuated, and cooled under vacuum before exposing to air. The promoter was subsequently added in a 1:1 atomic ratio with ruthenium by impregnation of Ru/MgO with aqueous cesium nitrate (Aldrich, 99.999%), barium nitrate (Aldrich, 99.999%), or lanthanum nitrate (Aldrich, 99.99%). Lastly, each sample was heated to 723 K in flowing N_2. All catalysts (Cs–Ru/MgO, Ba–Ru/MgO, La–Ru/MgO, and the unpromoted catalyst Ru/MgO) were crushed and sieved between 250 and 425 μm.

2.2. Adsorption of dihydrogen

The procedures used for dihydrogen chemisorption are provided elsewhere [41]. Briefly, a sample was heated under vacuum at 2 K min^{-1} to 673 K, reduced in flowing dihydrogen for 30 min, evacuated, and cooled under vacuum. The chemisorption isotherm was measured at 308 K. Turnover frequencies and the total number of active sites were based on the number surface Ru atoms counted by total hydrogen chemisorption (extrapolated to zero pressure) assuming an H/Ru_{surf} ratio of unity.

2.3. High-pressure reaction studies

The system used for evaluation of the catalysts was a fixed-bed, single-pass, tubular reactor operating between 1 and 20.7 atm total pressure. Approximately 1 g of catalyst was loaded into the reactor. The reactant gases consisted of dinitrogen (BOC, 99.999%), dihydrogen (BOC, 99.999%), and sometimes helium (BOC, 99.999%). The appropriate gas composition was first passed over a bed of MnO_2/SiO_2 and molecular sieves to remove trace amounts of dioxygen and water before exposure to the catalyst. The products were analyzed by an online gas chromatograph with a Porapak N column and a TCD detector. The TCD peak areas were calibrated by operating the catalyst at equilibrium and using the equilibrium concentrations determined by Larson and Dodge [44]. A more detailed description of the calibration procedure can be found in [12].

Each catalyst was evaluated at a total pressure of 20.7 atm and between 598 and 723 K under conditions close to and far from equilibrium. The ratio of dinitrogen to dihydrogen was changed from 1:3 to 3:1 (total flow rate of 400 ml min^{-1}) under conditions far from equilibrium in order to find the orders of reaction in dinitrogen and dihydrogen. Ammonia inhibition was evaluated by varying the total flow rate of reactants from 100 to 400 ml min^{-1}. Each of the catalysts was evaluated at elevated pressures for several days and no deactivation was observed.

2.4. Kinetic Model 1

According to Mechanism 1, the following rate expression can be derived,

$$\text{rate} = \frac{k_3[*]_o\{[N_2] - \frac{[NH_3]^2}{[H_2]^3 K_p}\}}{[1 + (\frac{k_1[H_2]}{k_2})^{1/2} + \frac{[NH_3]}{[H_2]^{3/2}}(\frac{k_3}{K_p k_4})^{1/2}]^2}, \quad (3)$$

where K_p is the overall equilibrium constant and $[*]_o$ is the total number of sites titrated by dihydrogen chemisorption (see Table 1). Rate constants were assumed to have an Arrhenius form. The preexponential factors for k_2 and k_4 (associative desorption of dihydrogen and dinitrogen, respectively) were assumed to be known, and independent of promoter.

Hinrichsen and co-workers determined through temperature-programmed desorption experiments that the preexponential factor for k_4 (associative desorption of N_2) was 2×10^{10} s^{-1} for both Ru/MgO and Cs–Ru/MgO [16,17]. In addition, they found with their optimization routine that the preexponential factor for k_2 (associative desorption of H_2) was 2.3×10^{13} s^{-1}. We inserted these constants into our model since they appeared to be independent of promoter.

Table 1
Properties of MgO-supported Ru catalysts

Catalyst	Ru (wt%)	Promoter (wt%)	Mol promoter/ mol Ru	H/Ru_{tot}
Ru/MgO	1.66	–	–	0.77
Cs–Ru/MgO	1.64	2.04	0.95	0.52
Ba–Ru/MgO	1.40	2.39	1.26	0.15
La–Ru/MgO	1.59	2.11	0.97	0.17

The number of unknown kinetic parameters was five: the rate constant for dihydrogen adsorption (k_1), the enthalpy for dihydrogen adsorption ($-\Delta H_{H_2ads}$), the preexponential factor for dinitrogen adsorption (k_3^o), the activation energy for dinitrogen adsorption (Ea_3), and the activation energy for dinitrogen desorption (Ea_4). A minimization of the following objective function was then carried out (within reasonable limits) using a Mathematica routine,

$$\text{SSE} = \sum_{i=1}^{N} (f_{N_2 calc} - f_{N_2 exp})^2, \quad (4)$$

where N was the total number of data sets for the catalyst, while $f_{N_2 calc}$ and $f_{N_2 exp}$ were the fractional conversion of dinitrogen calculated by the model and experimentally determined, respectively. The reactor was modeled as 8 CSTRs in series since a large portion of the data had conversions that were greater than 20% toward equilibrium. Based on correlations given in Levenspiel, a Peclet number of approximately 2 was calculated for the tubular reactor system [45]. Since some backmixing was present in the reactor bed, 8 CSTRs in series was considered to be a reasonable model of our system. Moreover, the relative change in the optimized kinetic parameters was small upon addition of more CSTRs.

2.5. Kinetic Model 2

Mechanism 2 was used to develop a more sophisticated kinetic model. In contrast to Model 1, no rate-determining step was assumed in Mechanism 2 and a variety of species (N, H, NH, NH_2, and NH_3) were allowed to occupy surface sites. The site balance on the surface is

$$[*]_o = [*] + [N*] + [H*] + [NH*] + [NH_2*] + [NH_3*], \quad (5)$$

where $[*]_o$ is the total number of surface sites and $[*]$ is the total number of unoccupied sites. Again, the reactor was modeled as a series of 8 CSTRs. As with Model 1, the relative change in the optimized kinetic parameters was small with the inclusion of additional CSTRs. The steady-state approximation was applied for each CSTR. In other words, the

Table 2
Rate constants used for Model 2 (the values are from a similar microkinetic model for Cs–Ru/MgO by Hinrichsen and co-workers [16] and they did not change with choice of basic promoter[a])

Rate constant	Preexponential factor	Activation energy
k_1[b]	Fitted	–
k_2	2.3×10^{13} atm^{-1} s^{-1}	Fitted
k_3	Fitted	Fitted
k_4	2.0×10^{10} s^{-1}	Fitted
k_5	6.0×10^{13} s^{-1}	86.5 kJ mol^{-1}
k_6	2.8×10^{14} s^{-1}	41.2 kJ mol^{-1}
k_7	4.7×10^{13} s^{-1}	60.4 kJ mol^{-1}
k_8	1.8×10^{13} s^{-1}	8.6 kJ mol^{-1}
k_9	3.3×10^{13} s^{-1}	17.2 kJ mol^{-1}
k_{10}	Fitted	Fitted
k_{11}	5.9×10^{13} s^{-1}	83.7 kJ mol^{-1}
k_{12}[b]	2.1×10^{8} atm^{-1} s^{-1}	–

[a] The rate constant for dihydrogen adsorption, the preexponential factor for dinitrogen adsorption, and the activation energies for hydrogen desorption, dinitrogen adsorption, and nitrogen desorption were all fitted using our Mathematica routine. The rate constant for reverse equation (2e) (k_{10}) was determined from the overall equilibrium constant.

[b] Ammonia adsorption and dihydrogen adsorption are assumed to be nonactivated.

concentrations of reactive intermediates in each CSTR were small and independent of time,

$$\frac{\mathrm{d}[x]}{\mathrm{d}t} = 0, \tag{6}$$

where $[x]$ is the concentration of a reactive intermediate. Therefore, seven highly nonlinear equations were solved for each CSTR.

Rate constants were assumed to have an Arrhenius form and the same five kinetic parameters were allowed to vary among catalysts: k_1, $-\Delta H_{\mathrm{H_2ads}}$, k_3^{o}, $E\mathrm{a}_3$, and $E\mathrm{a}_4$. With the exception of k_{10}, the rest of the kinetic parameters were fixed at the values provided by Hinrichsen et al. (see Table 2) for a microkinetic model associated with Cs–Ru/MgO [16]. The rate constant for the reverse step of equation (2e) (k_{10}) was determined from the overall equilibrium constant and the five fitted kinetic parameters. Attempts were made to use k_{11} or k_{12} to achieve thermodynamic consistency; however, these efforts were unsuccessful. As with Model 1, a Mathematica routine was used to minimize the objective function [equation (4)].

3. Results

Table 1 summarizes the properties of the catalysts [41]. The amounts of Ru and promoter in all of the catalysts were similar to the nominal values anticipated from the synthesis procedure. The unpromoted catalyst (Ru/MgO) revealed the highest H_2 chemisorption capacity. Addition of promoters lowered the dihydrogen uptake, which could be the result of a partial covering of the metal surface with the promoter or aggregation of Ru into larger particles. At this time we cannot ascertain which is the likely cause. Other researchers have used TPD, volumetric chemisorption, microkinetic modeling, TEM and XRD to show that both are possible for the Ru/MgO and Cs–Ru/MgO system [26,46]. Nevertheless, the results from dihydrogen chemisorption were used to calculate the turnover frequency (TOF) based on outlet ammonia pressure at each condition.

Table 3
Turnover frequencies (TOF) of ammonia synthesis over Ru catalysts supported on MgO UNDER stoichiometric conditions, 673 K, and 20.7 atm

Catalyst	TOF[a] (s^{-1})	TOF[b] (s^{-1})	Ea[c] (kJ mol^{-1})
Ru/MgO	3.76×10^{-3}	3.12×10^{-3}	107
Cs–Ru/MgO	3.35×10^{-2}	3.11×10^{-2}	111
Ba–Ru/MgO	1.46×10^{-1}	1.68×10^{-1}	96
La–Ru/MgO	1.06×10^{-1}	1.19×10^{-1}	86

[a] Based on total hydrogen chemisorption and calculated at a constant flow rate of 400 cm^3 min^{-1}.

[b] Based on total hydrogen chemisorption and calculated at a constant ammonia pressure of 0.1 atm.

[c] Activation energy calculated at a constant ammonia pressure of 0.1 atm.

Table 4
Orders of reaction for ammonia synthesis over Ru catalysts supported on MgO at 20.7 atm[a]

Catalyst	Temperature (K)	α (N_2)	β (H_2)	γ (NH_3)
Ru/MgO	648	0.88	−0.74	0.05
Cs–Ru/MgO	598	0.87	−1.01	0.09
Ba–Ru/MgO	623	0.84	−0.37	−0.14
La–Ru/MgO	623	0.85	−0.15	−0.17

[a] Where the rate expression is $r = k P_{\mathrm{N_2}}^{\alpha} P_{\mathrm{H_2}}^{\beta} P_{\mathrm{NH_3}}^{\gamma}$.

Table 3 summarizes the observed turnover frequencies measured at 673 K and stoichiometric conditions at constant flow (measured) and constant ammonia pressure of 0.1 atm (calculated). Addition of base promoters improved the catalytic activity of Ru/MgO by at least an order of magnitude. Moreover, the activities of La–Ru/MgO and Ba–Ru/MgO were almost an order of magnitude greater than Cs–Ru/MgO under these conditions. The TOF measured at constant flow and constant ammonia pressure were similar, indicating weak dependence of the rate on NH_3 (see Table 4).

The temperature dependence of the observed rate is also summarized in Table 3. The apparent activation energy for Cs–Ru/MgO was 111 kJ mol^{-1}, which is consistent with the values reported in the literature [11,12,19,26]. The apparent activation energy is reduced with promotion by Ba and especially La, and parallels the trend in dihydrogen order of reaction. The catalysts did not deactivate with time on stream.

Reaction orders are summarized in Table 4. In all cases, the ammonia synthesis reaction was approximately first order in N_2 and zero order in NH_3. Fig. 1 shows graphically an example of the dependence of the rate on dihydrogen, dinitrogen and ammonia. The order of reaction in H_2 depended on the choice of promoter. The results illustrated in Fig. 2

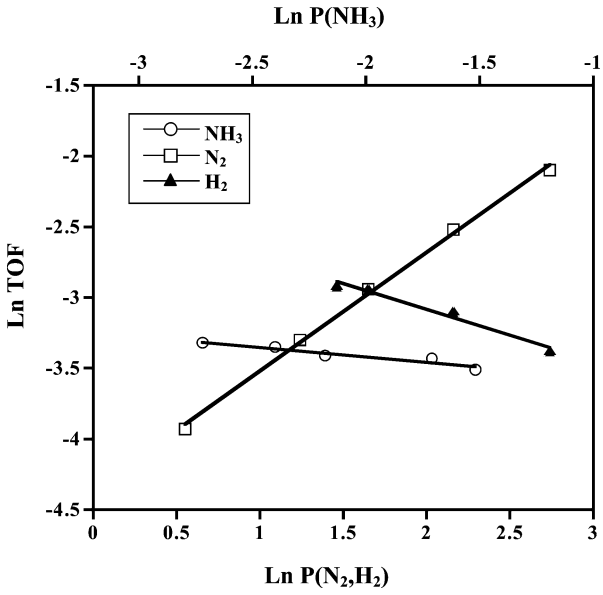

Fig. 1. Dependence of the turnover frequency (s^{-1}) on the partial pressures (atm) of N_2, H_2, and NH_3 at 20.7 atm total pressure and 623 K over La–Ru/MgO. The total flow rate was varied from 100 to 400 ml min^{-1} in order to determine the order in NH_3 at stoichiometric reaction conditions. Each reactant partial pressure was varied while holding the other constant at 5.2 atm.

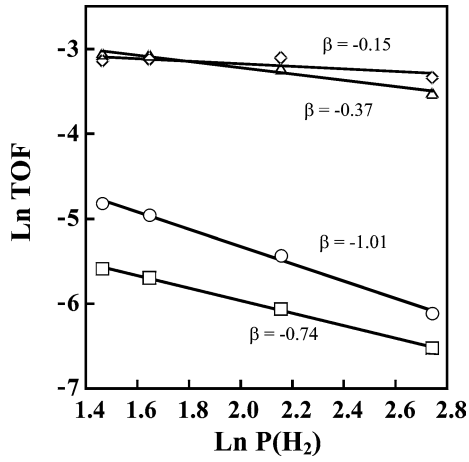

Fig. 2. Effect of promoter on the experimentally determined dihydrogen order of reaction (β) at 20.7 atm total pressure where Ru/MgO (□) is at 648 K, Cs–Ru/MgO (◯) is at 598 K, Ba–Ru/MgO (△) is at 623 K, and La–Ru/MgO (◇) is at 623 K. Dihydrogen partial pressure was varied while holding the dinitrogen partial pressure constant at 5.2 atm.

and Table 4 indicated a very weak dependence of the rate on H_2 for Ba- and La-promoted Ru/MgO. These results are consistent with the literature [11,12,26] as well as with previous results in our laboratory at 3 atm [41].

3.1. Model 1

Table 5 presents the optimized kinetic parameters for Mechanism 1. This model suggests that the enthalpy of dihydrogen adsorption ($-\Delta H_{H_2ads}$) and the activation energy of dinitrogen dissociation (Ea_3) are significantly affected by the choice of promoter. Examining the parameters for La- and Cs-promoted catalysts shows that the enthalpy for dihydrogen adsorption changes by 32 kJ mol^{-1} and the activation energy for dinitrogen dissociation changes by 26 kJ mol^{-1}. Moreover, there is a trade-off between a lower barrier for dinitrogen dissociation and a larger enthalpy for dihydrogen adsorption. The activation energy for step 4, the associative desorption of N atoms, varies to a lesser extent than either $-\Delta H_{H_2ads}$ or Ea_3. The model also indicates that the preexponential factor for dinitrogen dissociation for the unpromoted Ru/MgO is 5 to 10 times smaller than the base-promoted catalysts.

Table 5
Fitted kinetic parameters from Model 1

Catalyst	k_1 (atm^{-1} s^{-1})	$-\Delta H_{H_2ads}$ (kJ mol^{-1})	k_3^o (atm^{-1} s^{-1})	Ea_3 (kJ mol^{-1})	Ea_4 (kJ mol^{-1})
Ru/MgO	4.75×10^7	98.5	997	28.2	147
Cs–Ru/MgO	5.55×10^7	100	5710	24.5	132
Ba–Ru/MgO	9.15×10^6	82.8	14000	45.8	135
La–Ru/MgO	2.83×10^7	68.2	7960	50.9	133

A comparison of calculated ammonia pressures from the optimized model and experimentally determined ammonia pressures are shown for La–Ru/MgO in Fig. 3a. Analogous plots for the other catalysts are similar (not shown). Fig. 3b shows that for La–Ru/MgO the model is able to predict the ammonia pressures far from and close to equilibrium. Equilibrium is indicated when the ammonia pressure decreased with increasing temperature.

3.2. Model 2

Table 6 presents the optimized kinetic parameters for Mechanism 2. Because this model was sensitive to starting conditions, the output of Model 1 was used as the input to Model 2. As summarized in Table 6, the enthalpy of dihydrogen adsorption ($-\Delta H_{H_2ads}$) and the activation energy of dinitrogen dissociation (Ea_3) were affected by the choice of promoter. However, the magnitude of the changes was less than that found with Model 1. Nevertheless, the Cs–Ru/MgO catalyst had the lowest barrier for dinitrogen dissociation and a largest enthalpy for dihydrogen adsorption. The activation energy for step 4, the associative desorption of N atoms, varied to a lesser extent than either $-\Delta H_{H_2ads}$ or Ea_3. The model also predicts a preexponential factor for dinitrogen dissociation for Ru/MgO that was 5 to 10 times smaller than the base-promoted catalysts.

Figs. 4a and 4b show (for Cs–Ru/MgO) that the model represents the data well under all conditions studied. Analogous plots for the other catalysts were similar (not shown).

3.3. Sensitivity of Model 1

Figs. 5a and 5b show that Model 1 can reliably determine $-\Delta H_{H_2ads}$. Here $-\Delta H_{H_2ads}$ was modified by ±10 kJ mol^{-1} while each of the other four kinetic parameters (k_1, k_3^o, Ea_3,

Table 6
Fitted kinetic parameters from Model 2

Catalyst	k_1 ($\text{atm}^{-1}\,\text{s}^{-1}$)	$-\Delta H_{\text{H}_2\text{ads}}$ (kJ mol^{-1})	k_3^{o} ($\text{atm}^{-1}\,\text{s}^{-1}$)	$E\text{a}_3$ (kJ mol^{-1})	$E\text{a}_4$ (kJ mol^{-1})	k_{10}^{o} [a] (s^{-1})	$E\text{a}_{10}$ [a] (kJ mol^{-1})
Ru/MgO	4.75×10^7	98.5	996	27.9	146	3.89×10^{12}	44.9
Cs–Ru/MgO	4.80×10^7	102	6400	23.7	129	3.95×10^{12}	46.1
Ba–Ru/MgO	7.03×10^6	88.6	16300	39.6	133	8.97×10^{11}	72.1
La–Ru/MgO	2.38×10^7	82.7	9220	37.7	135	4.20×10^{12}	79.0

[a] These columns were used to achieve thermodynamic consistency.

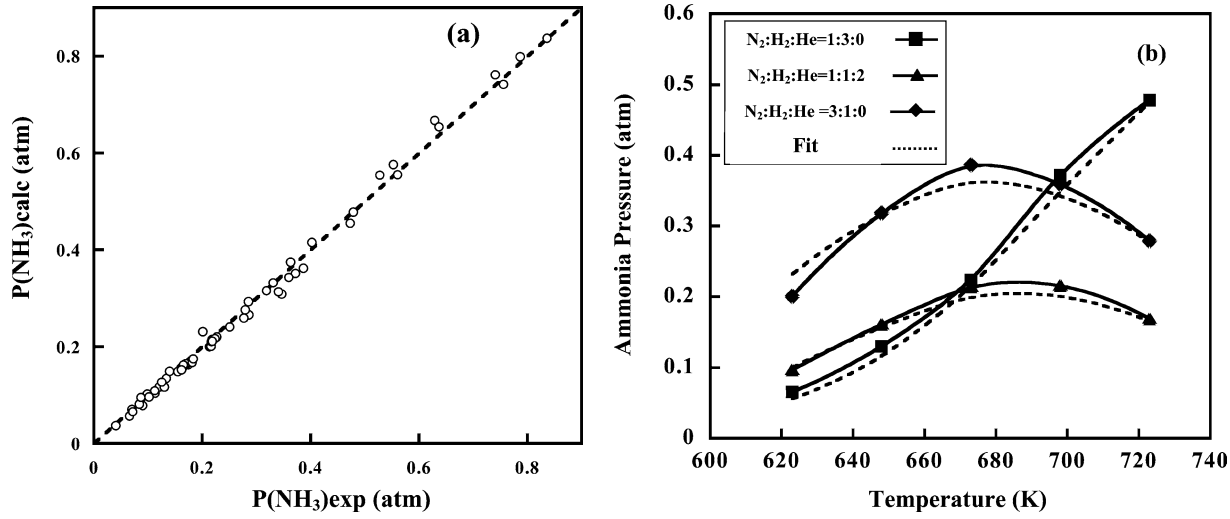

Fig. 3. (a) Comparison of calculated and experimentally determined ammonia outlet pressures over La–Ru/MgO from Model 1 at 20.7 atm. (b) Comparison of calculated and experimentally determined ammonia outlet pressures as a function of temperature over La–Ru/MgO from Model 1 at 20.7 atm. All data from figure (a) were used to determine the fits in figure (b); however, only data at some of the ratios of reactants are reported for clarity.

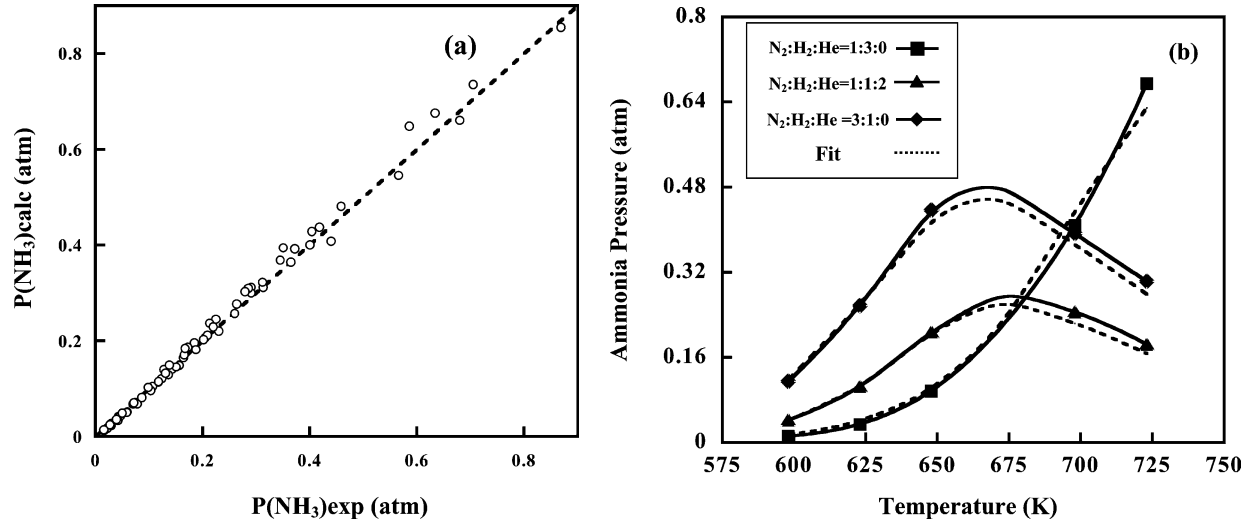

Fig. 4. (a) Comparison of calculated and experimentally determined ammonia outlet pressures over Cs–Ru/MgO from Model 2 at 20.7 atm. (b) Comparison of calculated and experimentally determined ammonia outlet pressures as a function of temperature over Cs–Ru/MgO from Model 2 at 20.7 atm. All data from figure (a) were used to determine the fits in figure (b); however, only data at some of the ratios of reactants are reported for clarity.

and $E\text{a}_4$) were fixed at those for the lowest SSE. The quality of the fit is significantly affected by this change.

Figs. 6a and 6b show in a different way that Model 1 can reliably determine $-\Delta H_{\text{H}_2\text{ads}}$, $E\text{a}_3$, and $E\text{a}_4$. In this case, $-\Delta H_{\text{H}_2\text{ads}}$ was modified while each of the other four kinetic parameters (k_1, k_3^{o}, $E\text{a}_3$, and $E\text{a}_4$) were optimized with the Mathematica routine [equation (4)]. For La–Ru/MgO, $-\Delta H_{\text{H}_2\text{ads}}$ was modified by $\pm 30\ \text{kJ mol}^{-1}$. A minimum in the total sum of squared error was clearly reached at $71\ \text{kJ mol}^{-1}$. Additionally, the activation energy for de-

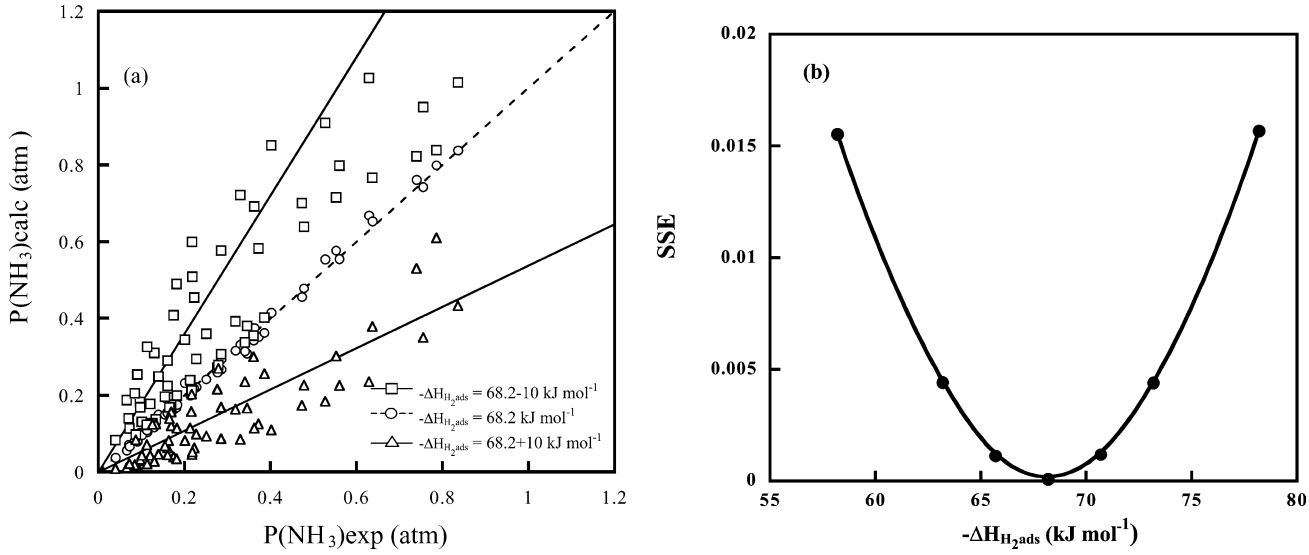

Fig. 5. (a) Comparison of calculated and experimental ammonia pressures over La–Ru/MgO from Model 1, with $-\Delta H_{\mathrm{H_2ads}} = 68.2 \pm 10$ kJ mol^{-1}. For each of the three cases, $-\Delta H_{\mathrm{H_2ads}}$ as well as the other four kinetic parameters (k_1, k_3^o, Ea_3, and Ea_4) were fixed. (b) Comparison of sum of squares over La–Ru/MgO from Model 1 with $-\Delta H_{\mathrm{H_2ads}} = 68.2 \pm 10$ kJ mol^{-1}. For each case, $-\Delta H_{\mathrm{H_2ads}}$ as well as the other four kinetic parameters (k_1, k_3^o, Ea_3, and Ea_4) were fixed.

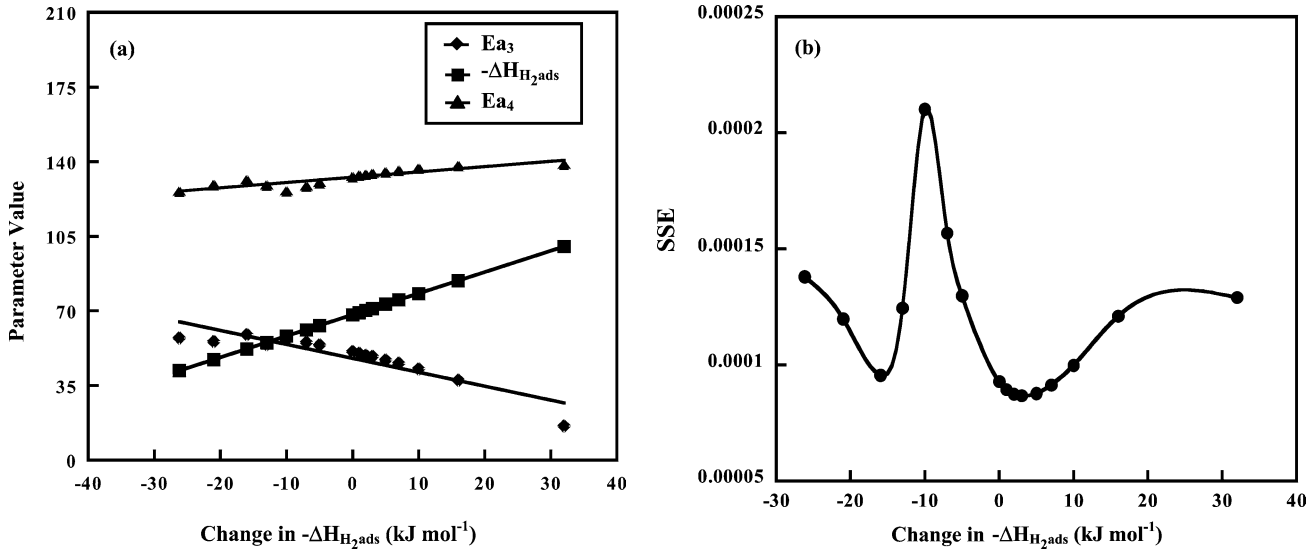

Fig. 6. (a) Effect of changing $-\Delta H_{\mathrm{H_2ads}}$ on the activation energies of dinitrogen adsorption and desorption for La–Ru/MgO with Model 1. Here $-\Delta H_{\mathrm{H_2ads}}$ was fixed for each optimization while each of the other four kinetic parameters (k_1, k_3^o, Ea_3, and Ea_4) were allowed to float. (b) Effect of the enthalpy of adsorption of dihydrogen on the quality of the fit (SSE) for La–Ru/MgO with Model 1. Here $-\Delta H_{\mathrm{H_2ads}}$ was fixed for each optimization while each of the other four kinetic parameters (k_1, k_3^o, Ea_3, and Ea_4) were allowed to float.

sorption of N_2 is less affected by the change in the heat of hydrogen adsorption than Ea_3 (activation energy for dinitrogen dissociation). The sensitivity of the SSE to changes in the fitted parameters indicates that the observed effect of promoter on the values of $-\Delta H_{\mathrm{H_2ads}}$ and Ea_3 is real.

4. Discussion

Numerous researchers have determined that a small percentage of the surface Ru atoms are involved in the dissociation of N_2 [18,19,47,48]. A model by Dahl et al. for $Ru/MgAl_2O_4$ assumed that only 9% of the surface Ru atoms are active for dissociation [29]. Therefore, our assumption that all of the exposed Ru atoms counted by total dihydrogen chemisorption ($[*]_o$) needs to be addressed. Reducing the total number of sites by 90% increases the preexponential factor for dinitrogen dissociation so that the product $k_3^o [*]_o$ is virtually constant. Neither the quality of the fits nor the other four fitted kinetic parameters changed significantly by changing the total site density.

Table 7
Effect of promoter on the calculated coverages of reactive intermediates from Model 2 at the outlet of the reactor at 648 K, 20.7 atm, N_2:H_2 = 1:3, and a constant ammonia pressure of 0.1 atm

Catalyst	∗	N∗	NH∗	NH_2∗	NH_3∗	NH_x∗[a]	H∗
MgO	0.02	0.02	5.3×10^{-5}	4.9×10^{-7}	0.04	0.06	0.92
Cs–Ru/MgO	0.01	0.01	4.2×10^{-5}	5.2×10^{-7}	0.03	0.04	0.95
Ba–Ru/MgO	0.09	0.04	1.6×10^{-5}	2.3×10^{-8}	0.17	0.21	0.70
La–Ru/MgO	0.08	0.04	1.6×10^{-5}	2.4×10^{-8}	0.15	0.19	0.73

[a] Where NH_x is the total coverage of nitrogen-containing species.

Hinrichsen and co-workers used N_2 isotopic exchange and temperature-programmed experiments to determine the kinetics of dinitrogen adsorption and desorption on Ru/MgO and Cs–Ru/MgO, and our optimization results are in reasonable agreement with their findings [17]. For Ru/MgO, Hinrichsen et al. reported the preexponential factor and the activation energy for dinitrogen dissociation to be 5700 $atm^{-1}\,s^{-1}$ and 40–61 $kJ\,mol^{-1}$, respectively [17]. For Cs–Ru/MgO (with a 1:1 molar ratio of Cs:Ru), the preexponential factor and the activation energy for dinitrogen dissociation were 5700 $atm^{-1}\,s^{-1}$ and 33 $kJ\,mol^{-1}$, respectively [17].

Results from both of our models suggest that the effect of base promotion of Ru/MgO on ammonia synthesis rates is a trade-off between a higher enthalpy of dihydrogen adsorption ($-\Delta H_{H_2ads}$) and a lower activation barrier for dinitrogen dissociation (Ea_3). This implies that the H and N atoms are competing for the same sites. The coverages of intermediates calculated from Model 2 are shown in Table 7. Catalysts that are strongly inhibited by dihydrogen (Cs–Ru/MgO and Ru/MgO) have surface coverages of H atoms exceeding 90%. However, Ba- and La-promoted catalysts are less inhibited by dihydrogen and therefore have lower surface coverages of H atoms. Aika et al. reported previously that alkali addition to supported Ru promotes the dissociation of dinitrogen and the retardation by hydrogen [13].

Many researchers have attempted to measure $-\Delta H_{H_2ads}$ on Ru catalysts. Single-crystal studies have shown that $-\Delta H_{H_2ads}$ varies from 35 to 125 $kJ\,mol^{-1}$ [49–53]. Narayan and co-workers determined that it is 90 $kJ\,mol^{-1}$ for strongly held hydrogen and 50 $kJ\,mol^{-1}$ for weakly held hydrogen on Ru/SiO_2 [54]. In addition, K and Ag did not affect $-\Delta H_{H_2ads}$ for strongly held hydrogen [54]. Zupanc et al. studied Ru/MgO and found the it to be 70–123 $kJ\,mol^{-1}$ [46]. Our results from kinetic modeling are within the reported values.

It is logical to suggest that the most active ammonia synthesis catalysts are those that minimize the activation barrier for dinitrogen dissociation (Ea_3) since it is the likely rate-determining step [12,16]. Therefore, we were rather surprised to find that both models predict Ea_3 to be significantly smaller for Ru/MgO than Ba–Ru/MgO and La–Ru/MgO given that Ba and La promotion increased activity. The small preexponential factor, k_3^o, for dinitrogen dissociation for Ru/MgO is suggested to be the cause. We expect that k_3^o and Ea_3 are highly coupled and that an overestimation of the total number of sites available has reduced k_3^o significantly. In addition, the unpromoted catalyst may have a lower fraction of Ru sites capable of N_2 dissociation, which will be reflected in a lower value of k_3^o.

Table 8
Isotopic transient results at 673 K, 3 atm, 40 $ml\,min^{-1}$, and N_2:H_2 = 1:3 [41]

Catalyst	P_{NH_3} (atm)	TOF_{global}[a] ($10^{-4}\,s^{-1}$)	TOF_{intr}[b] ($10^{-4}\,s^{-1}$)	θ_{NH_x}[c]
Ru/MgO	0.0026	13.6	244	0.056
Cs–Ru/MgO	0.0095	64.1	1250	0.051
Ba–Ru/MgO	0.0039	54.2	500	0.108
La–Ru/MgO	0.0052	75.3	526	0.143

[a] Where TOF_{global} is calculated from the exit ammonia concentration normalized by the number of surface Ru atoms determined by hydrogen chemisorption.

[b] TOF_{intr} is the intrinsic TOF determined from the residence time of nitrogen-containing surface intermediates. No assumption about the number of active sites is required for this calculation.

[c] Where θ_{NH_x} is the total coverage of nitrogen-containing species and is based on total hydrogen chemisorption.

Table 7 shows that the most abundant nitrogen-containing species is ammonia, regardless of the promoter. However, decreasing the activation energy in step 5 increased the coverage of NH species without altering the quality of the fit. Therefore, Model 2 cannot determine confidently which of the nitrogen containing species is most prevalent on the surface. Coverages obtained from the microkinetic model of Dahl et al. show that NH is the most abundant N-containing species with NH_2 also present in significant amounts. Model 1 assumes that N atoms are the most abundant N-containing intermediates on the surface and the optimized parameters show the same trend as those of Model 2. The advantage of using Model 2 is its ability to calculate the coverage of all nitrogen-containing intermediates.

In a recent paper, we describe the use of isotopic transient analysis to evaluate these same Cs-, Ba-, and La-promoted Ru/MgO catalysts [41]. We showed that the global turnover frequencies of Cs, Ba-, and La-promoted catalysts were very similar (Table 8) at 3 atm total pressure. The weak dependence of the rate on dihydrogen for the La- and Ba-promoted catalysts may be a result of the greater effect of total pressure on the global turnover frequency. It also may be a result of lateral interactions. In addition, both the isotopic transient experiments and the kinetic models agree that the coverage of nitrogen containing species (NH_x = N, NH, NH_2, and

NH_3) is small on each of the catalysts. Moreover, the two methods indicate a significant increase in the coverage of NH_x for Ba- and La-promoted Ru/MgO compared to Cs–Ru/MgO.

We have also recently determined the apparent activation barrier at 3 atm for each of the promoted catalysts via isotopic transient analysis [41]. The activation energies for Cs–Ru/MgO, Ba–Ru/MgO, and La–Ru/MgO were 28, 45, and 50 kJ mol^{-1}, respectively [41]. They closely match the activation barriers for dinitrogen dissociation determined from the two models reported here. Since the rate-determining step in ammonia synthesis is the dissociation of dinitrogen, all other steps in the reaction sequence involving adsorbed nitrogen are at quasi-equilibrium. Thus the apparent activation energy determined from isotopic transient analysis is related to the barrier for dinitrogen dissociation. Care must be exercised when interpreting results from isotopic transient analysis since the equilibrium constants for the quasi-equilibrated steps are also temperature dependent.

Stoltze derived expressions for the orders of reaction in ammonia synthesis that are solely functions of coverages of surface intermediates [55]. The expressions were based on the rate of ammonia synthesis being equal to the forward rate of dinitrogen dissociation [55]. The coverages determined from Model 2 give predicted dihydrogen orders of −0.86, −0.92, −0.58, and −0.61 for Ru/MgO, Cs–Ru/MgO, Ba–Ru/MgO, and La–Ru/MgO, respectively. These values follow about the same trend as that observed in Table 4.

A significant role of dihydrogen is also seen in alkane hydrogenolysis over Pt. According to Koningsberger and co-workers, the choice of support affects the order of reaction in dihydrogen as well as the apparent activation energy of alkane hydrogenolysis over supported Pt [56]. The more acidic the support, the weaker the inhibition by dihydrogen and the smaller the apparent activation energy. The authors used X-ray absorption near-edge spectroscopy at the Pt L_2 and L_3 edges to show that hydrogen prefers the atop Pt site on acidic supports while it prefers the 3-fold Pt site on basic supports. Density-functional theory calculations of H adsorbed on Pt clusters showed that $-\Delta H_{H_2ads}$ is significantly higher on catalysts with less acidic supports. Thus the coverage of H atoms on Pt is smaller on the more acidic supported catalysts. Apparently, the alkane hydrogenolysis reaction is affected to a large extent by the strength of the Pt–H bond.

5. Conclusions

The kinetics of high-pressure ammonia synthesis showed that promotion of Ru/MgO with Ba or La lowered the inhibition by dihydrogen. Promotion of Ru/MgO with Cs increased the inhibition by dihydrogen. Two different mechanisms were used to successfully model the experimental results close to and far from equilibrium at 20.7 atm total pressure. Each model revealed a correlation between a lower activation barrier for dinitrogen dissociation and a higher $-\Delta H_{H_2ads}$. Thus, base promotion of Ru/MgO involves a trade-off between a faster intrinsic rate of N_2 dissociation and greater competition for active sites with adsorbed H atoms. One of the models predicted trends in NH_x coverage that were measured with isotopic transient analysis.

Acknowledgments

This work was supported by the National Science Foundation (Grant CTS-9729812) and the Department of Energy (Basic Energy Sciences, Grant DE-FG02-95ER14549). The authors acknowledge Dr. John Monnier from Eastman Chemical Company for dihydrogen chemisorption and Ru elemental analysis.

References

[1] K. Aika, K. Tamaru, in: A. Nielsen (Ed.), Ammonia Catalysis and Manufacture, vol. 1, Springer, Berlin, 1995, p. 104.
[2] Chementator, Chem. Engr. 3 (1993) 19.
[3] P.J. Goethel, R.T. Yang, J. Catal. 111 (1988) 220.
[4] R. Baker, Carbon 24 (1986) 715.
[5] C.J.H. Jacobsen, Chem. Commun. (2000) 1057.
[6] S. Murata, K.-I. Aika, J. Catal. 136 (1992) 118.
[7] K. Aika, A. Ohya, A. Ozaki, Y. Inoue, I. Yasumori, J. Catal. 92 (1985) 305.
[8] K.-I. Aika, T. Takano, S.J. Murata, J. Catal. 136 (1992) 126.
[9] D. Szmigiel, H. Bielawa, M. Kurtz, O. Hinrichsen, M. Muhler, W. Rarog, S. Jodzis, Z. Kowalczyk, L. Znak, J. Zielinski, J. Catal. 205 (2002) 205.
[10] B.C. McClaine, R.J. Davis, J. Catal. 210 (2002) 387.
[11] T. Becue, R.J. Davis, J.M. Garces, J. Catal. 179 (1998) 129.
[12] B.C. McClaine, T. Becue, C. Lock, R.J. Davis, J. Mol. Catal A: Chem. 163 (2000) 105.
[13] K. Aika, M. Kumasaka, T. Oma, O. Kato, H. Matsuda, N. Watanabe, K. Yamazaki, A. Ozaki, T. Onishi, Appl. Catal. 28 (1986) 57.
[14] C.T. Fishel, R.J. Davis, J.M. Garces, J. Catal. 163 (1996) 148.
[15] Y. Izumi, M. Hoshikawa, K. Aika, Bull. Chem. Soc. Jpn. 67 (1994) 3191.
[16] O. Hinrichsen, F. Rosowski, M. Muhler, G. Ertl, Chem. Eng. Sci. 51 (1996) 1683.
[17] O. Hinrichsen, F. Rosowski, A. Hornung, M. Muhler, G. Ertl, J. Catal. 165 (1997) 33.
[18] H. Bielawa, O. Hinrichsen, A. Birkner, M. Muhler, Angew. Chem. Int. Ed. 40 (2001) 1061.
[19] Y. Niwa, K.-I. Aika, Res. Chem. Int. 24 (1998) 593.
[20] Y. Niwa, K.-I. Aika, J. Catal. 162 (1996) 138.
[21] S. Murata, K.-I. Aika, T. Onishi, Chem. Lett. (1990) 1067.
[22] Y. Niwa, K.-I. Aika, Chem. Lett. (1996) 3.
[23] Y. Izumi, Y. Iwata, K.-I. Aika, J. Phys. Chem. 100 (1996) 9421.
[24] Y. Kadowaki, K.-I. Aika, J. Catal. 161 (1996) 178.
[25] W. Rarog, Z. Kowalczyk, J. Sentek, D. Skladanowski, J. Zielinski, Catal. Lett. 68 (2000) 163.
[26] F. Rosowski, A. Hornung, O. Hinrichsen, D. Herein, M. Muhler, G. Ertl, Appl. Catal. A 151 (1997) 443.
[27] S.E. Siporin, B.C. McClaine, S.L. Anderson, R.J. Davis, Catal. Lett. 81 (2002) 265.
[28] B.C. McClaine, R.J. Davis, J. Catal. 211 (2002) 379.
[29] S. Dahl, J. Sehested, C.J.H. Jacobsen, E. Tornqvist, I. Chorkendorff, J. Catal. 192 (2000) 391.

[30] I. Rossetti, N. Pernicone, L. Forni, Appl. Catal. 208 (2001) 271.
[31] T.W. Hansen, J.B. Wagner, P.L. Hansen, S. Dahl, H. Topsoe, C.J.H. Jacobsen, Science 294 (16) (2001) 1508.
[32] W. Rarog-Pilecka, D. Szmigiel, Z. Kowalczyk, S. Jodzis, J. Zielinski, J. Catal. 218 (2003) 465.
[33] K.-I. Aika, T. Kawahara, S. Murata, T. Onishi, Bull. Chem. Soc. Jpn. 63 (1990) 1221.
[34] Z. Zhong, K.-I. Aika, Inorg. Chim. Acta 280 (1998) 183.
[35] Z. Zhong, K.-I. Aika, Chem. Commun. (1997) 1223.
[36] Z. Zhong, K.-I. Aika, J. Catal. 173 (1998) 535.
[37] L. Forni, D. Molinari, I. Rossetti, N. Pernicone, Appl. Catal. A 185 (1999) 269.
[38] C. Liang, Z. Wei, Q. Xin, C. Li, Appl. Catal. A 208 (2001) 193.
[39] Z. Kowalczyk, S. Jodzis, W. Raróg, J. Zieliński, J. Pielaszek, Appl. Catal. A 173 (1998) 153.
[40] T.W. Hansen, P.L. Hansen, S. Dahl, C.J.H. Jacobsen, Catal. Lett. 84 (2002) 7.
[41] S.E. Siporin, R.J. Davis, J. Catal. 222 (2004) 315.
[42] S. Hagen, R. Barfod, R. Fehrmann, C.J.H. Jacobsen, H.T. Teunissen, I. Chorkendorff, J. Catal. 214 (2003) 327.
[43] S.E. Siporin, R.J. Davis, W. Raróg-Pilecka, D. Szmigiel, Z. Kowalczyk, Catal. Lett. 93 (2004) 61.
[44] A.T. Larson, R.L. Dodge, J. Am. Chem. Soc. 45 (1923) 2918.
[45] O. Levenspiel, Chemical Reaction Engineering, third ed., Wiley, New York, 1999.
[46] C. Zupanc, A. Hornung, O. Hinrichsen, M. Muhler, J. Catal. 209 (2002) 501
[47] S. Dahl, E. Tornqvist, I. Chorkendorff, J. Catal. 192 (2000) 381.
[48] S. Dahl, A. Logadottir, R.C. Egeberg, J.H. Larsen, I. Chorkendorff, E. Tornqvist, J.K. Norskov, Phys. Rev. Lett. 83 (1999) 1814.
[49] P. Feulner, D. Menzel, Surf. Sci. 154 (1985) 465.
[50] G. Lauth, E. Schwartz, K. Christmann, J. Chem. Phys. 91 (1989) 3729.
[51] J.A. Schwarz, Surf. Sci. 87 (1979) 525.
[52] H. Shimizu, K. Christmann, G. Ertl, J. Catal. 61 (1980) 412.
[53] L. Danielson, M. Dresser, E. Donaldson, J. Dickinson, Surf. Sci. 71 (1978) 599.
[54] R.L. Narayan, N. Savargaonkar, M. Pruski, T.S. King, Stud. Surf. Sci. Catal. 101 (1996) 921.
[55] P. Stoltze, Phys. Scripta 36 (1987) 824.
[56] D.C. Koningsberger, M.K. Oudenhuijzen, J. de Graaf, J.A. van Bokhoven, D.E. Ramaker, J. Catal. 216 (2003) 178.